Electronic Supplementary Information

Rational design of hybridized local and charge transfer emitters towards high-performance fluorescent blue OLEDs

Shuxin Wang,[a,b] Hanlin Li,[c] Zhen Song,[d] He Jiang,[a,b] Xiandi Zhang,[a] Chui-Shan Tsang,[a] Quanlin Liu,[d] Lawrence Yoon Suk Lee,[a] Dongge Ma*[c] and Wai-Yeung Wong*[a,b]

[a]Department of Applied Biology and Chemical Technology and Research Institute for Smart Energy, The Hong Kong Polytechnic University, Hung Hom, Hong Kong, P. R. China

[b]The Hong Kong Polytechnic University Shenzhen Research Institute, Shenzhen 518057, P. R. China

[c]State Key Laboratory of Luminescent Materials and Devices, Center for Aggregation-Induced Emission, South China University of Technology, Guangzhou 510640, China

[d]The Beijing Municipal Key Laboratory of New Energy Materials and Technologies, School of Materials Sciences and Engineering, University of Science and Technology Beijing, Beijing 100083, China

Email: lawrence.ys.lee@polyu.edu.hk (Lawrence Yoon Suk Lee); msdgma@scut.edu.cn (Dongge Ma); wai-yeung.wong@polyu.edu.hk (Wai-Yeung Wong)

Table of Contents

ESI-1. Literature Research

Table S1. Critical parameters for the EL performance of OLEDs using anthracene-based blue HLCT emitters with $CIE_y \leq 0.12$.

Devices	λ_{EL}[a] (nm)	CIE (x, y)	EQE[b] (%)	$\eta_{roll\text{-}off}$[c] (%)	V_{on}[d] (V)	CE[e] (cd A^{-1})	PE[f] (lm W^{-1})	Ref.
PICNAnCz	448	(0.16,0.11)	9.05	13	4.4	9.07	5.76	1
CBP:PIAnTPh	440	(0.15,0.06)	8.09	11.4	3.3	6.97	5.89	2
CBP:PyIAnTPh	440	(0.15,0.07)	8.44	9.80	3.1	7.36	7.21	2
CBP:Icz-An-PPI	448	(0.15, 0.08)	4.59	35	3.6	5.83	5.08	3
CBP:IP-An-PPI	446	(0.15, 0.12)	7.51	4.5	3.1	7.61	7.66	3
mPAC	448	(0.16, 0.09)	6.76	14	4.3	5.61	3.48	4
DPEPO:PABP	456	(0.15,0.11)	6.31	-	4.1	5.85	4.65	5
DPEPO:PAIDO	452	(0.15,0.09)	8.82	-	3.7	7.64	7.27	5
DPIAPPB	472	(0.15, 0.12)	4.15	-	2.3	6.56	6.16	6
CADPPI	467	(0.15, 0.10)	4.78	-	2.3	9.85	10.84	6
PPI-An-NPPI	456	(0.15,0.11)	7.75	1.8	3.5	7.68	6.89	7
PPI-An-NPIM	449	(0.14,0.10)	7.48	4.5	3.5	7.17	6.44	7

[a] EL emission peak. [b] Maximum external quantum efficiency. [c] Efficiency roll-off at the practical brightness of 1000 cd m^{-2}. [d] Turn-on voltage at the luminance of 1 cd m^{-2}. [e] Maximum current efficiency. [f] Maximum power efficiency.

Table S2. Critical parameters for the EL performance of OLEDs with triphenylamine-anthracene-based blue HLCT emitters.

Devices	λ_{EL}[a] (nm)	CIE (x, y)	EQE[b] (%)	$\eta_{roll\text{-}off}$[c] (%)	V_{on}[d] (V)	CE[e] (cd A^{-1})	PE[f] (lm W^{-1})	Ref.
TPAAnPI	470	(0.15, 0.22)	11.47	15	3.4	18.09	12.35	8
TPAAnTAZ	484	(0.20, 0.38)	5.56	0.2	2.8	12.5	10.7	9
CBP:TPA-AN-NA	460	(0.14, 0.16)	5.44	-	3.3	7.16	6.09	10
CBP:TPA-AN-TFP	468	(0.14, 0.20)	3.38	-	3.6	5.17	4.16	10
DPIAPPB	472	(0.15, 0.12)	4.15	-	2.3	6.56	6.16	6
CBP:mTAHPI	463	(0.14, 0.17)	6.73	57	2.8	-	8.1	11
CBP:pTAHPI	472	(0.15, 0.23)	8.13	59	2.8	-	10.39	11
CBP:pTAPI	467	(0.19, 0.25)	3.13	78	3.2	-	4.72	11

[a] EL emission peak. [b] Maximum external quantum efficiency. [c] Efficiency roll-off at the practical brightness of 1000 cd m^{-2}. [d] Turn-on voltage at the luminance of 1 cd m^{-2}. [e] Maximum current efficiency. [f] Maximum power efficiency.

References

1 X. Lv, L. Xu, Y. Yu, W. Cui, H. Zhou, M. Cang, Q. Sun, Y. Pan, S. Xue and W. Yang, *Chem. Eng. J.*, 2021, **408**, 127333.

2 F. Liu, Z. Cheng, L. Wan, L. Gao, Z. Yan, D. Hu, L. Ying, P. Lu and Y. Ma, *Chem. Eng. J.*, 2021, **426**, 131351.

3 X. Zheng, T. Huang, G. Yang, A. Lin, K. Chen, X. Chen, J. Li and Q. Tong, *Chem. Eur. J.*, 2021, **27**, 16181–16188.

4 Y. Xu, X. Liang, Y. Liang, X. Guo, M. Hanif, J. Zhou, X. Zhou, C. Wang, J. Yao, R. Zhao, D. Hu, X. Qiao, D. Ma and Y. Ma, *ACS Appl. Mater. Interfaces*, 2019, **11**, 31139–31146.

5 Y. Xu, C. Wang, X. Zhou, J. Zhou, X. Guo, X. Liang, D. Hu, F. Li, D. Ma and Y. Ma, *J. Phys. Chem. Lett.*, 2019, **10**, 6878–6884.
6 J. Jayabharathi, V. Thanikachalam, R. Ramya and S. Panimozhi, *RSC Adv.*, 2019, **9**, 33693–33709.
7 B. Liu, Z.-W. Yu, D. He, M.-D. Li, W.-F. Xie and Q.-X. Tong, *Mater. Today Chem.*, 2022, **23**, 100630.
8 X. Lv, M. Sun, L. Xu, R. Wang, H. Zhou, Y. Pan, S. Zhang, Q. Sun, S. Xue and W. Yang, *Chem. Sci.*, 2020, **11**, 5058–5065.
9 F. Liu, X. Man, H. Liu, J. Min, S. Zhao, W. Min, L. Gao, H. Jin and P. Lu, *J. Mater. Chem. C*, 2019, **7**, 14881–14888.
10 J. Zhang, Y. Zhao, H. Xu, D. Zhang, Y. Miao, R. Shinar, J. Shinar, H. Wang, B. Xu and Y. Wu, *J. Mater. Chem. C*, 2019, **7**, 10810–10817.
11 W. Li, P. Chasing, W. Benchaphanthawee, P. Nalaoh, T. Chawanpunyawat, C. Kaiyasuan, N. Kungwan, S. Namuangruk, T. Sudyoadsuk and V. Promarak, *J. Mater. Chem. C*, 2021, **9**, 497–507.

ESI-2. Synthesis and Characterization

All the reagents and solvents used for the synthesis were purchased from commercial suppliers and used without further purification.

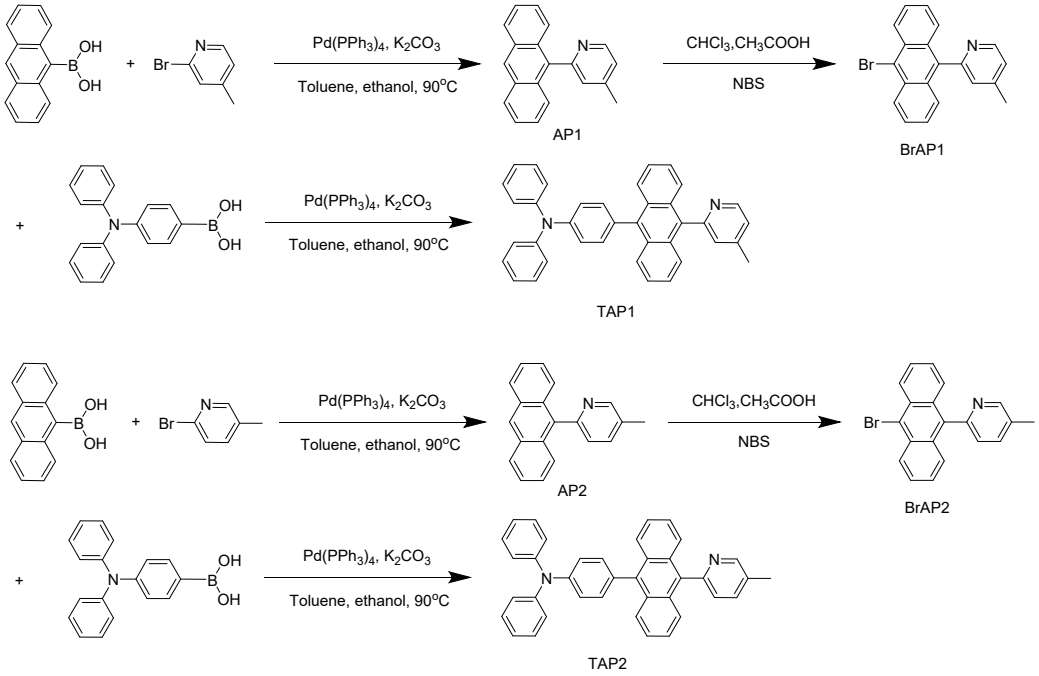

Scheme S1. The synthetic routes for TAP1 and TAP2.

Anthracene-9-ylboronic acid (AP1)

AP1 was synthesized by the Suzuki coupling reaction. $Pd(PPh_3)_4$ (288.89 mg, 0.25

mmol), 2-bromo-4-methylpyridine (860 mg, 5 mmol), 9-Anthraceneboronic acid (1.65 g, 7.5 mmol), K_2CO_3 (2 M, 50 mL), ethanol (50 mL), and toluene (150 mL) were added into the 500 mL flask. The reaction mixture was heated at 90℃ for 12 h under an argon atmosphere. The solvents were evaporated under vacuum and the resulting residue was extracted with ethyl acetate and washed with deionized water. The organic phase was collected, dried with Na_2SO_4, and then evaporated to dryness. The crude product was purified by silica gel chromatography (hexane: dichloromethane = 1: 1) to give a yellow solid (1.03 g, 76.2%). ^{1}H NMR (400 MHz, Chloroform-*d*) δ (ppm): 8.77 (d, *J* = 5.1 Hz, 1H), 8.53 (s, 1H), 8.05 (d, *J* = 8.4 Hz, 2H), 7.59 (d, *J* = 8.7 Hz, 2H), 7.48 – 7.43 (m, 2H), 7.40 – 7.34 (m, 3H), 7.28 (d, *J* = 4.7 Hz, 1H), 2.49 (s, 3H).

2-(10-Bromoanthracen-9-yl)-4-methylpyridine (BrAP1)

AP1 (1.35 g, 5 mmol) was dissolved in chloroform (50 mL) and acetic acid (15 mL). N-Bromosuccinimide (978.9 mg, 5.5 mmol) was added slowly. The reaction mixture was stirred at room temperature for 4 h before quenching with water. The product was extracted with CH_2Cl_2 twice. The organic phase was collected, dried with Na_2SO_4, and then evaporated to dryness with a rotary evaporator. The crude product was purified by silica gel chromatography (hexane: dichloromethane = 1: 1) to give a yellow solid (1.29 g, 73.9%). ^{1}H NMR (400 MHz, Chloroform-*d*) δ (ppm): 8.76 (d, *J* = 5.1 Hz, 1H), 8.61 (d, *J* = 8.9 Hz, 2H), 7.61 – 7.52 (m, 4H), 7.40 (ddd, *J* = 8.8, 6.4, 1.2 Hz, 2H), 7.34 – 7.28 (m, 2H), 2.49 (s, 3H).

4-(10-(4-Methylpyridin-2-yl)anthracen-9-yl)-N,N-diphenylaniline (TAP1)

TAP1 was synthesized by the Suzuki coupling reaction. $Pd(PPh_3)_4$ (288.89 mg, 0.25 mmol), 2-(10-bromoanthracen-9-yl)-4-methylpyridine (1.74 g, 5 mmol), (4-(diphenylamino)phenyl)boronic acid (2.17 g, 7.5 mmol), K_2CO_3 (2 M, 50 mL), ethanol (50 mL), and toluene (150 mL) were added into the 500 mL flask. The reaction mixture was heated at 90℃ for 12 h under an argon atmosphere. The solvents were evaporated under vacuum and the resulting residue was extracted with ethyl acetate and washed with deionized water. The organic phase was collected, dried with Na_2SO_4, and then evaporated to dryness. The crude product was purified by silica gel chromatography (hexane: dichloromethane = 1: 1) to give a white solid (2.24 g, 87.5%). ^{1}H NMR (400 MHz, DMSO-d_6) δ (ppm): 8.68 (d, *J* = 5.0 Hz, 1H), 7.73 – 7.66 (m, 2H), 7.45 – 7.28 (m, 14H), 7.21 – 7.13 (m, 6H), 7.07 (t, *J* = 7.3 Hz, 2H), 2.41 (s, 3H). ^{13}C NMR (101 MHz, Chloroform-*d*) δ (ppm): 158.34, 149.82, 147.83, 147.55, 147.19, 137.94, 135.13, 132.64, 132.31, 131.94, 130.18, 129.80, 129.41, 127.71, 127.21, 126.23, 125.47, 124.96, 124.67, 123.40, 123.23, 123.09, 21.24. MALDI-TOF: m/z calcd for $C_{46}H_{26}$ $[M]^+$: 512.225, found: 512.480.

2-(Anthracen-9-yl)-4-methylpyridine (AP2)

AP2 was synthesized by the Suzuki coupling reaction. $Pd(PPh_3)_4$ (288.89 mg, 0.25

mmol), 2-bromo-5-methylpyridine (860 mg, 5 mmol), 9-anthraceneboronic acid (1.65 g, 7.5 mmol), K_2CO_3 (2 M, 50 mL), ethanol (50 mL), and toluene (150 mL) were added into the 500 mL flask. The reaction mixture was heated at 90℃ for 12 h under an argon atmosphere. The solvents were evaporated under vacuum and the resulting residue was extracted with ethyl acetate and washed with deionized water. The organic phase was collected, dried with Na_2SO_4, and then evaporated to dryness. The crude product was purified by silica gel chromatography (hexane: dichloromethane = 1: 1) to give a yellow solid (1.05 g, 78.3%). ^{1}H NMR (400 MHz, Chloroform-*d*) δ (ppm): 8.75 (s, 1H), 8.53 (s, 1H), 8.05 (d, *J* = 8.5 Hz, 2H), 7.73 (d, *J* = 7.9 Hz, 1H), 7.61 (d, *J* = 8.8 Hz, 2H), 7.45 (q, *J* = 7.0 Hz, 3H), 7.39 – 7.33 (m, 2H), 2.52 (s, 3H).

2-(10-Bromoanthracen-9-yl)-5-methylpyridine (BrAP2)

AP2 (1.35 g, 5 mmol) was dissolved in chloroform (50 mL) and acetic acid (15 mL). N-Bromosuccinimide (978.9 mg, 5.5 mmol) was added slowly. The reaction was stirred at room temperature for 4 h before quenching with water. The product was extracted with CH_2Cl_2 twice. The organic phase was collected, dried with Na_2SO_4, and then evaporated to dryness with a rotary evaporator. The crude product was purified by silica gel chromatography (hexane: dichloromethane = 1: 1) to give a yellow solid (1.31 g, 75.2%). ^{1}H NMR (400 MHz, Chloroform-*d*) δ (ppm): 8.74 (d, *J* = 2.2 Hz, 1H), 8.61 (d, *J* = 8.9 Hz, 2H), 7.73 (dd, *J* = 7.8, 2.3 Hz, 1H), 7.62 – 7.53 (m, 4H), 7.43 – 7.36 (m, 3H), 2.53 (s, 3H).

4-(10-(5-Methylpyridin-2-yl)anthracen-9-yl)-N,N-diphenylaniline (TAP2)

TAP2 was synthesized by the Suzuki coupling reaction. $Pd(PPh_3)_4$ (288.89 mg, 0.25 mmol), 2-(10-bromoanthracen-9-yl)-5-methylpyridine (1.74 g, 5 mmol), (4-(diphenylamino)phenyl)boronic acid (2.17 g, 7.5 mmol), K_2CO_3 (2 M, 50 mL), ethanol (50 mL), and toluene (150 mL) were added into the 500 mL flask. The reaction mixture was heated at 90℃ for 12 h under an argon atmosphere. The solvents were evaporated under vacuum and the resulting residue was extracted with ethyl acetate and washed with deionized water. The organic phase was collected, dried with Na_2SO_4, and then evaporated to dryness. The crude product was purified by silica gel chromatography (hexane: dichloromethane = 1: 1) to give a white solid (2.31 g, 90.2%). ^{1}H NMR (400 MHz, Dichloromethane-d_2) δ (ppm): 8.74 (s, 1H), 7.85 (d, *J* = 8.5 Hz, 2H), 7.77 (d, *J* = 7.9 Hz, 1H), 7.58 (d, *J* = 8.3 Hz, 2H), 7.45 – 7.25 (m, 17H), 7.09 (t, *J* = 7.3 Hz, 2H), 2.53 (s, 3H). ^{13}C NMR (101 MHz, Chloroform-*d*) δ (ppm): 155.53, 150.54, 147.84, 147.18, 137.93, 136.94, 135.01, 132.65, 132.30, 131.94, 131.86, 130.20, 129.93, 129.41, 127.22, 126.32, 126.25, 125.44, 124.96, 124.67, 123.23, 123.09, 18.46. MALDI-TOF: m/z calcd for $C_{46}H_{26}$ $[M]^+$: 512.225, found: 512.213.

ESI-3. Measurements

Instrumentation for structure characterization: ^{1}H and ^{13}C nuclear magnetic resonance (NMR) spectra were recorded on a Bruker Ultra Shield Plus 400 MHz instrument (400 MHz for ^{1}H and 101 MHz for ^{13}C, respectively) with dimethyl sulfoxide (DMSO)-d_6, dichloromethane (CH_2Cl_2)-d_2, or chloroform-*d* ($CDCl_3$) as the solvent and tetramethylsilane (TMS, δ = 0.00 ppm) as the internal standard. Molecular mass was determined by Bruker Ultraflextreme MALDI-TOF mass spectrometer. Single crystal X-ray diffraction data was collected using a Siemens Smart CCD diffractometer with graphite-monochromated MoKα radiation (λ = 0.71073 Å) at 298 (2) K. The crystal structure was solved by direct methods and refined with fullmatrix least-squares technique using the ShelXL (Sheldrick, 2015) and ShelXT (Sheldrick, 2015) programs, respectively.

Thermal stability measurements: Thermal properties of the deep-blue emitters were investigated by thermogravimetric analysis (TGA) and differential scanning calorimetry (DSC). TGA measurements were performed using a Perkin Elmer Pyris 6 under a nitrogen atmosphere with a heating rate of 10°C min^{-1} from 30-800°C. DSC analyses were performed on a Perkin Elmer Pyris Diamond DSC instrument under a nitrogen atmosphere with a heating rate of 10°C min^{-1}. Temperature at 5% weight loss was used as the decomposition temperature (T_d).

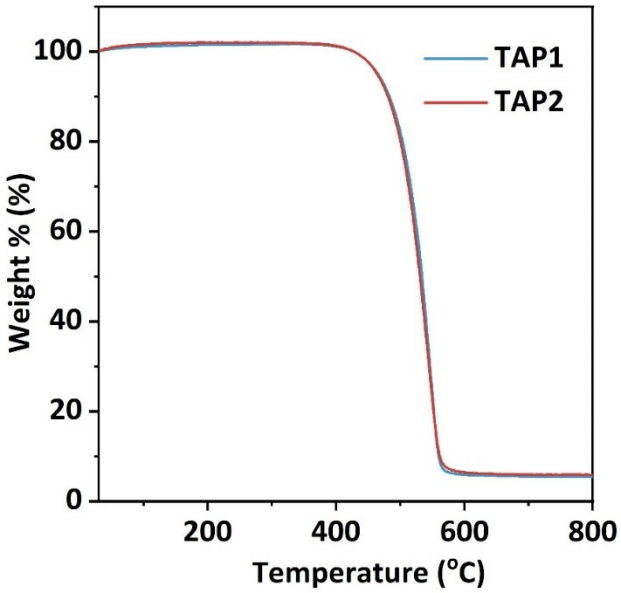

Figure S1. TGA curves of TAP1 and TAP2.

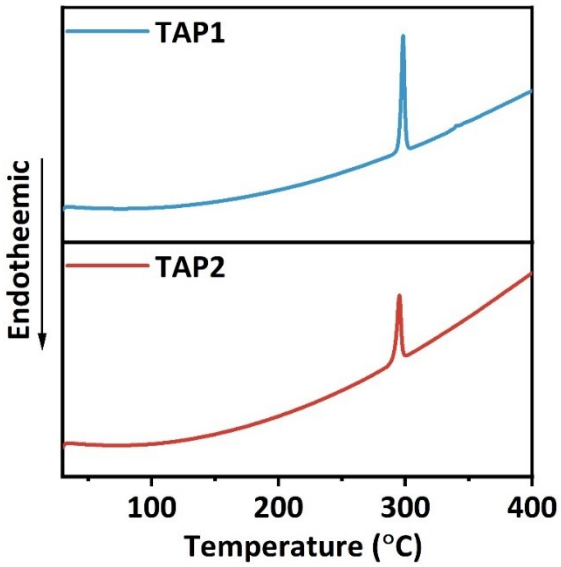

Figure S2. DSC curves of TAP1 and TAP2.

Electrochemical property measurements: Cyclic voltammetry (CV) measurements were performed at room temperature on a CHI660E system in a typical three-electrode cell with a working electrode (glass carbon), a reference electrode (Ag/Ag^+, referenced against ferrocene/ferrocenium (FOC), and a counter electrode (Pt wire) in acetonitrile solution of tetrabutylammonium hexafluorophosphate (Bu_4NPF_6) (0.1 M) at a sweeping rate of 100 mV s^{-1}. Highest occupied molecular orbital (HOMO) energy levels (E_{HOMO}) of the materials were estimated based on the reference energy level of ferrocene (4.8 eV below the vacuum) according to Equation S1:

$$E_{HOMO} = -\left(E_{onset}^{Ox} - E_{\left(Fc/Fc^{+}\right)} + 4.8\right) \text{ eV} \quad \text{(S1)}$$

where $E_{(Fc/Fc^+)}$ is the onset potential of oxidation wave of ferrocene (Fc) *vs* Ag/Ag^+ and E_{onset}^{Ox} is the onset potential of the oxidation wave of the materials deposited as thin films on the surface of the working electrode. The lowest unoccupied molecular orbital energy level (E_{LUMO}) was estimated by adding the optical bandgap (E_g) to the corresponding HOMO energy level.

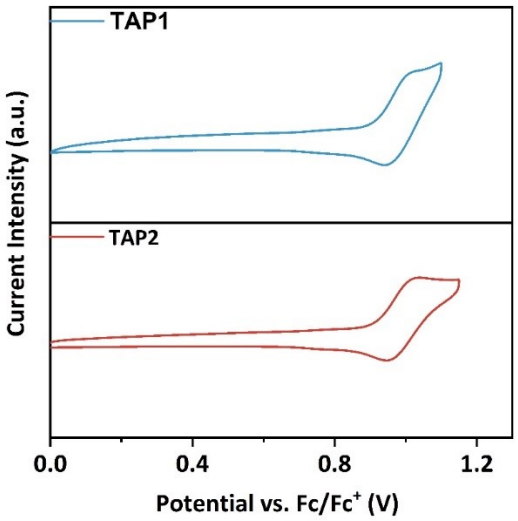

Figure S3. Cyclic voltammograms of TAP1 and TAP2.

Photophysical property measurements: Ultraviolet-visible (UV-Vis) spectra were recorded on a Varian Cary 4000 UV-Visible spectrophotometer. The photoluminescent (PL) spectra were obtained on an Fluoromax-4 spectrophotometer. Transient PL decay curves were collected using an Edinburgh FLS 1000 fluorescence spectrophotometer at room temperature using a laser of 375 nm as the excitation source. The absolute photoluminescence quantum yield (PLQY) was obtained on an Edinburgh FLS1000 fluorescence spectrophotometer with an integrating sphere. The relative photoluminescence quantum yield (PLQY) was obtained on an Fluoromax-4 spectrophotometer using 9,10-diphenylanthracene as a standard.

ESI-4. Solvatochromic Effect

The properties of ground state (S_0) and the lowest singlet excited state (S_1) can be better understood through solvatochromic experiment. One reliable way to explore the influence of solvent environment on the optical property of our sample is by using the Lippert-Mataga equation, a model that describes the interactions between the solvent and the dipole moment of solute:

$$hc(v_a - v_f) = hc(v_a^0 - v_f^0) - \frac{2(u_e - u_g)^2}{a^3} f(\varepsilon,n) \quad \text{(S2)}$$

where f is the orientational polarizability of solvents, μ_e is the dipole moment of excited state, μ_g is the dipole moment of ground state; a is the solvent cavity (Onsager) radius, derived from the Avogadro number (N), molecular weight (M), and density (d = 1.0 g cm^{-3}); ε and n are the solvent dielectric and the solvent refractive index, respectively. f(ε,n) and a can be calculated respectively as follows

$$f(\varepsilon, n) = \frac{\varepsilon - 1}{2\varepsilon + 1} - \frac{n^2 - 1}{2n^2 + 1} \quad \text{(S3)}$$

$$a = (3M/4N\pi d)^{1/3} \quad \text{(S4)}$$

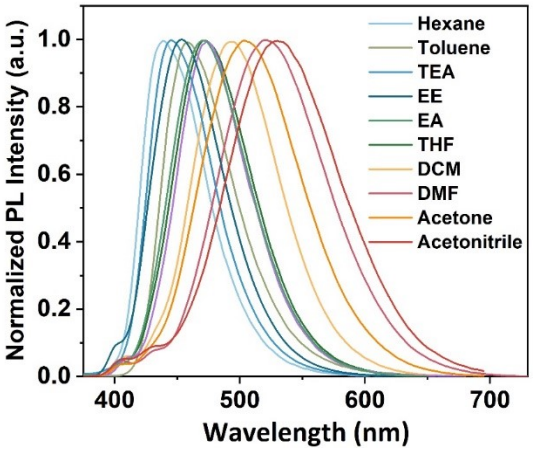

Figure S4. The PL spectra of TAP1 in different solvents under 355 nm excitation.

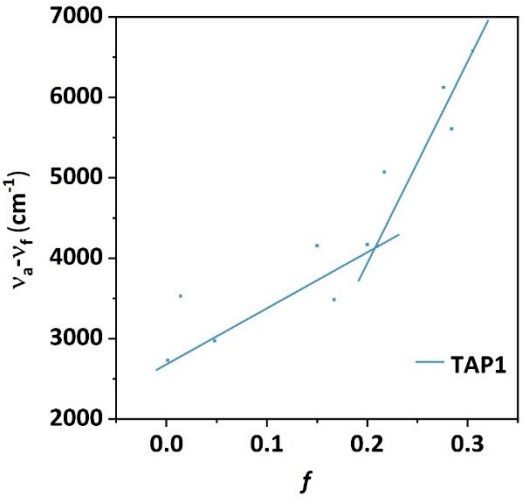

Figure S5. The solvatochromic Lippert-Mataga models of TAP1 under 355 nm excitation.

ESI-5. Theoretical Calculations

The density functional theory (DFT) calculations were conducted using ORCA software at the def2-TZVP basis set with def2/J and def2/JK as auxiliary basis set. For the purpose of investigating the properties of excited-states, natural transition orbitals (NTOs) of absorption were evaluated for the excited-states, involving both singlet and triplet states using time-dependent density functional theory (TD-DFT) at the def2-

TZVPP basis set with def2/J as auxiliary basis set.

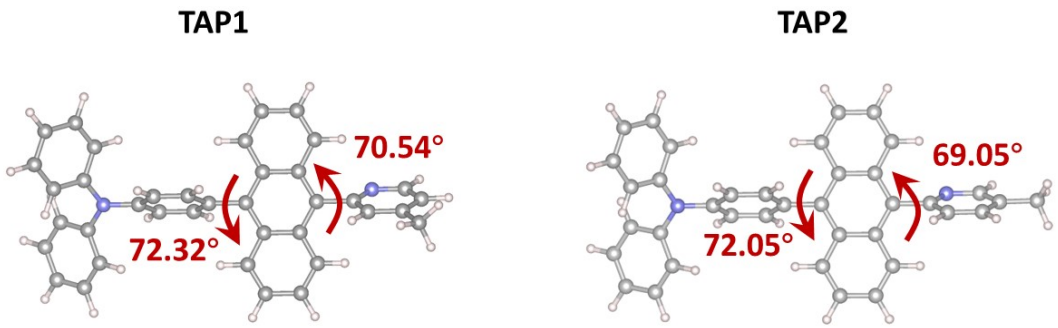

Figure S6. Optimized ground state geometries of TAP1 and TAP2.

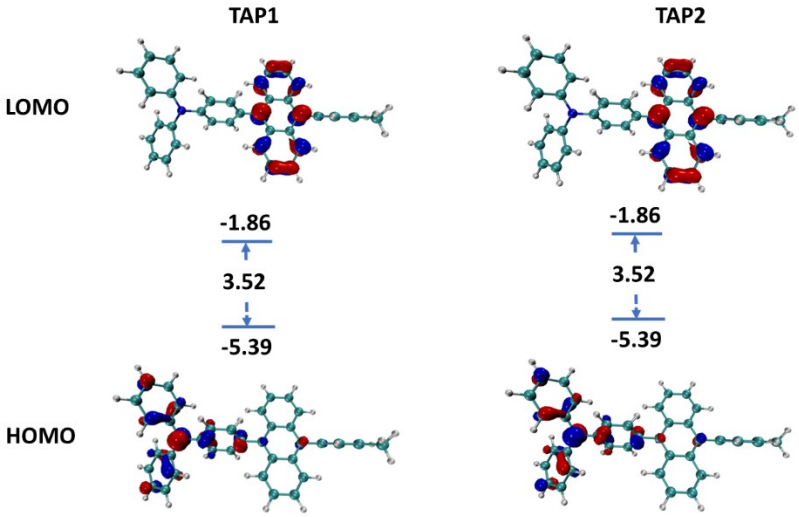

Figure S7. The spatial distributions of the molecular orbitals for TAP1 and TAP2.

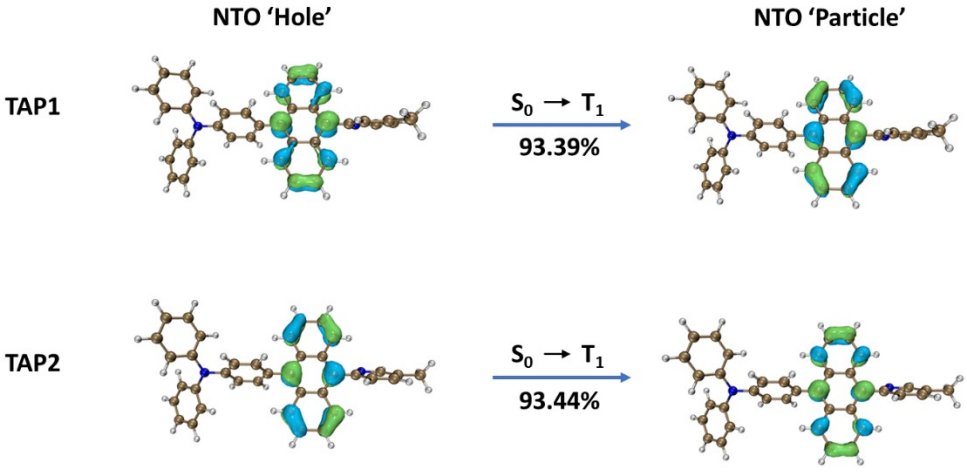

Figure S8. NTOs distributions for $S_0 \rightarrow T_1$ transition of TAP1 and TAP2.

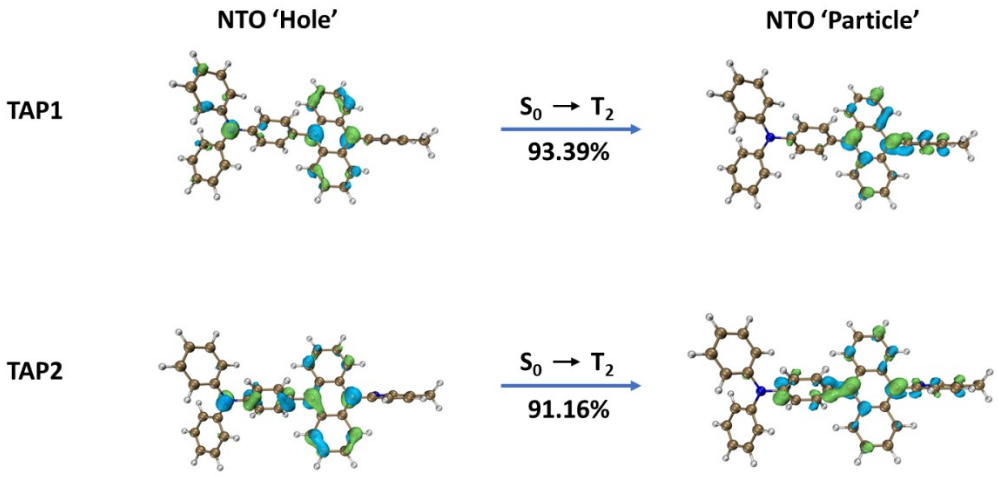

Figure S9. NTOs distributions for $S_0 \rightarrow T_2$ transition of TAP1 and TAP2.

ESI-6. Device Fabrication

Glass precoated with a 180 nm thick layer of indium tin oxide (ITO) was used as the device substrate, which has a sheet resistance of 10 Ω sq^{-1}. The ITO substrates were first ultrasonicated for 50 min and then cleaned with detergents and deionized water. Subsequently, all the substrates were dried in an oven at 120°C for 20 min, treated with UV-ozone for 4 min, and finally transferred into a high-vacuum evaporator (<1×10^{-5} Pa). All the organic materials were thermally evaporated onto the ITO substrates without breaking the vacuum. The current density-luminance-voltage properties were tested using a complete measurement system including a Keithley 2400 source meter and a LS-110 luminance meter. The EL spectra were collected using a Spectrascan PR650 spectrophotometer. The EQEs were calculated using the luminance intensity, current density, and EL spectra of the devices according to **Equation S5**.

$$EQE = \frac{\pi e \eta_{cd/A} \int \lambda p(\lambda) d\lambda}{hcK_m \int p(\lambda)\Phi(\lambda) d\lambda} \quad \text{(S5)}$$

where $\eta_{cd/A}$ is the current efficiency (cd/A); h is the Planck constant; c is the speed of light in vacuum; λ is the wavelength (nm); e is the electron charge; $p(\lambda)$ is the relative electroluminescent intensity at each wavelength; $\Phi(\lambda)$ is the Commission Internationale de l'Eclairage chromaticity (CIE) standard photopic luminous efficiency function; and K_m is a constant of 683 lm/W.

The exciton utilization efficiency EUE of OLEDs can be estimated according to the equation as below: EQE = (γ × EUE × Φ_{PL}) × η_{out} where γ is the recombination efficiency

of the injected electron and hole (generally identified as 100%); Φ_{PL} is the PLQY of the emitter; η_{out} is the light out-coupling fraction, which is estimated as 20%~30% for the glass substrates.

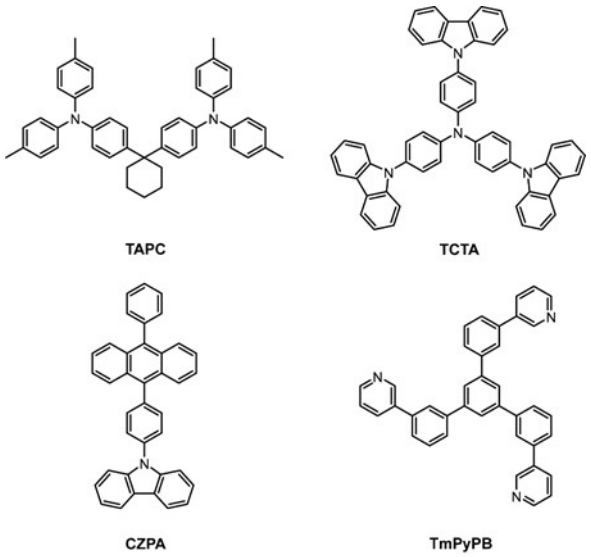

Figure S10. The molecular structures of the materials used in the deep-blue devices based on TAP1 and TAP2 emitters.

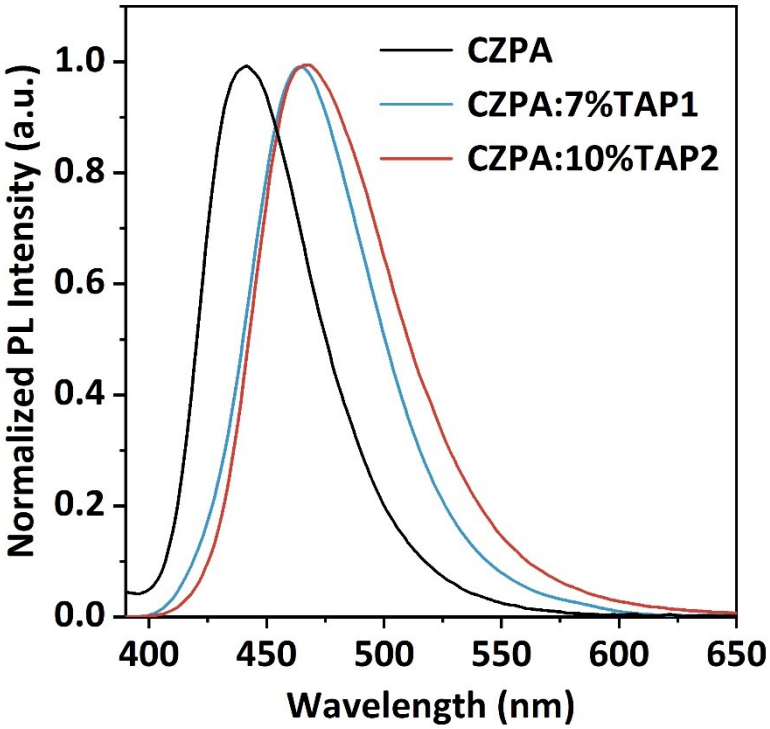

Figure S11. The PL spectra of the pure CZPA film, CZPA: 7% TAP1 film, and CZPA: 10% TAP2 film.

ESI-6. Nuclear Magnetic Resonance Spectra

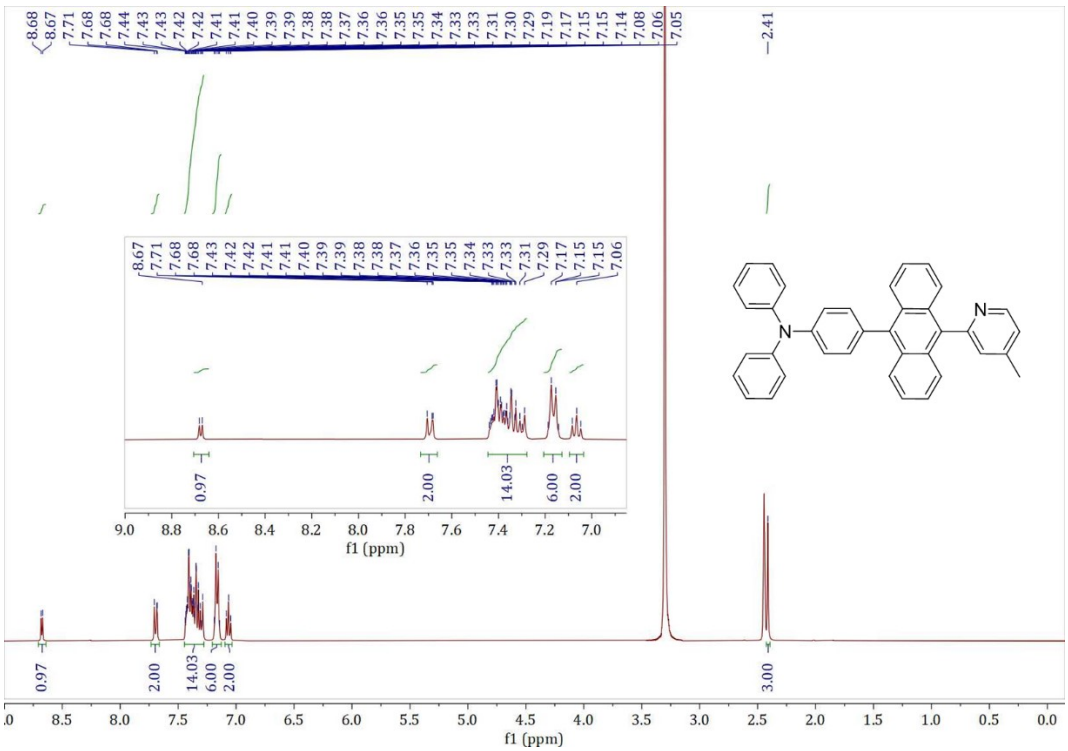

Figure S12. ^{1}H NMR spectrum of TAP1 in DMSO.

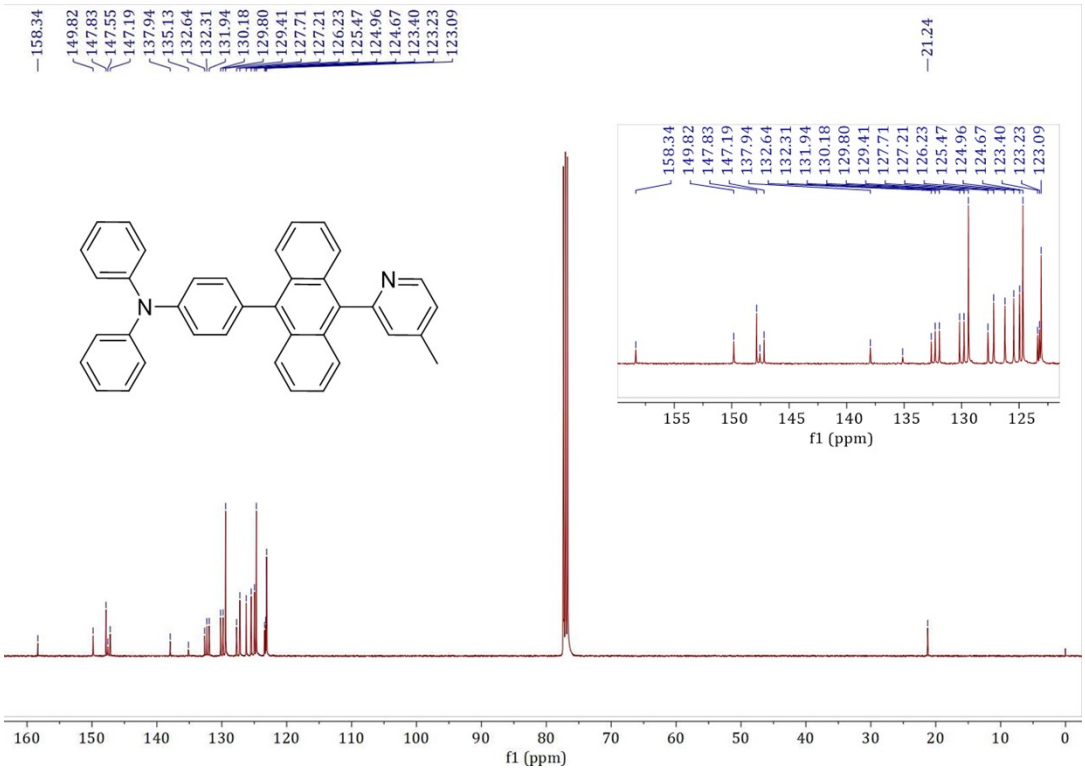

Figure S13. $^{13}C\{^{1}H\}$ NMR spectrum of TAP1 in $CDCl_3$.

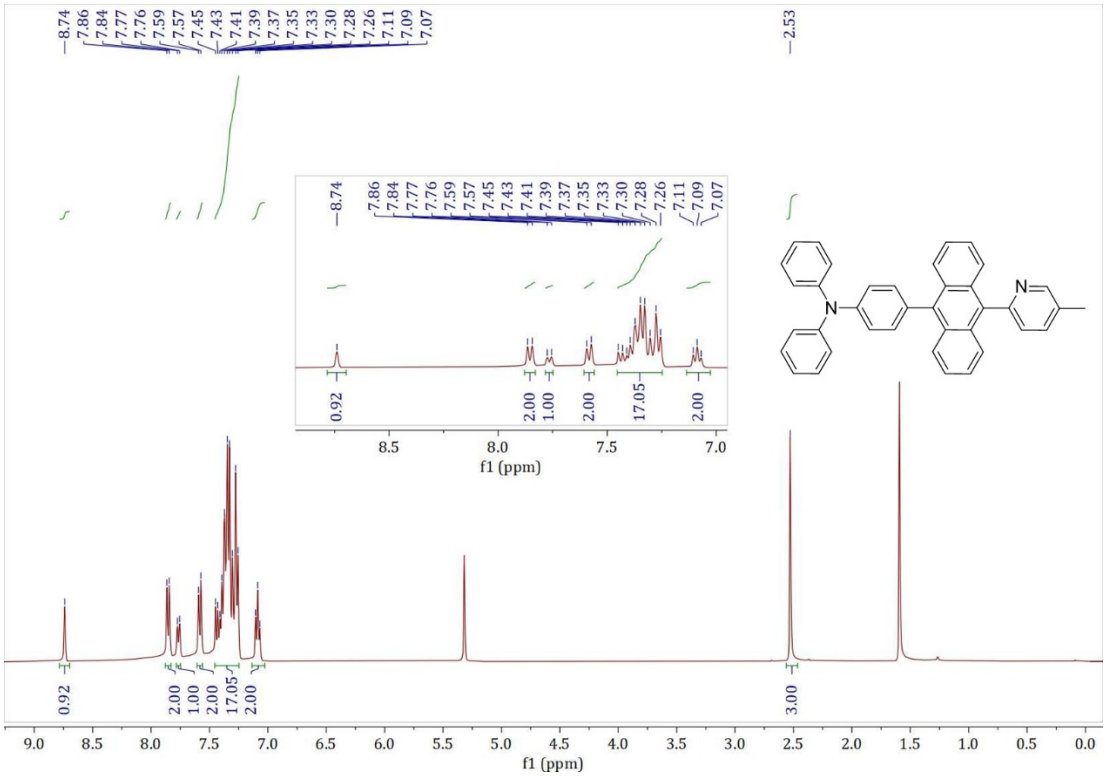

Figure S14. ^{1}H NMR spectrum of TAP2 in CH_2Cl_2

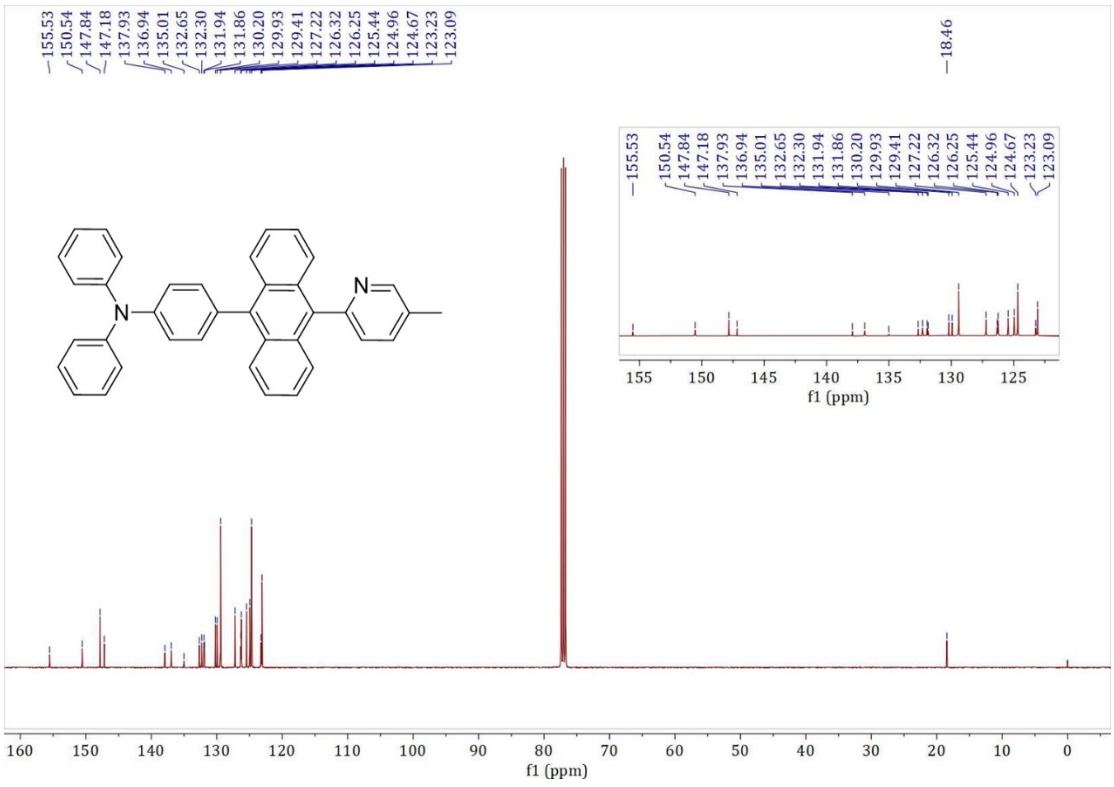

Figure S15. $^{13}C\{^{1}H\}$ NMR spectrum of TAP2 in $CDCl_3$.